ACS APPLIED NANO MATERIALS
Cite This: ACS Appl. Nano Mater. 2018, 1, 877−885
Article
www.acsanm.org

Tunable Assembly of Gold Nanorods in Polymer Solutions To Generate Controlled Nanostructured Materials

Ryan Poling-Skutvik,[†] Jonghun Lee,[‡] Suresh Narayanan,[‡] Ramanan Krishnamoorti,*[,†] and Jacinta C. Conrad*[,†]

[†]Department of Chemical and Biomolecular Engineering, University of Houston, Houston, Texas 77204-4004, United States
[‡]Advanced Photon Source, Argonne National Laboratory, Argonne, Illinois 60439, United States

Supporting Information

ABSTRACT: Gold nanorods grafted with short-chain polymers are assembled into controlled open structures using polymer-induced depletion interactions and structurally characterized using small-angle X-ray scattering. When the nanorod diameter is smaller than the radius of gyration of the depletant polymer, the depletion interaction depends solely on the correlation length of the polymer solution and not directly on the polymer molecular weight. As the polymer concentration increases, the stronger depletion interactions increasingly compress the grafted chains and push the gold nanorods closer together. By contrast, other structural characteristics such as the number of nearest neighbors and fractal dimension exhibit a nonmonotonic dependence on polymer concentration. These parameters are maximal at intermediate concentrations, which are attributed to a crossover from reaction-limited to diffusion-limited aggregation. The control over structural properties of anisotropic nanoscale building blocks demonstrated here will be beneficial to designing and producing materials *in situ* with specific direction-dependent nanoscale properties and provides a crucial route for advances in additive manufacturing.

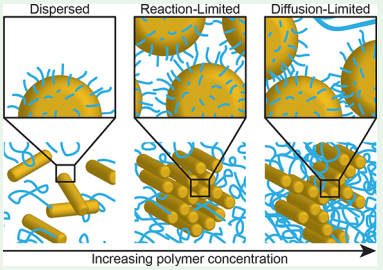

KEYWORDS: *depletion interactions, fractal structures, protein limit, small-angle X-ray scattering, ultraviolet−visible spectroscopy*

INTRODUCTION

Gold nanoparticles exhibit unique optical and electronic properties, advantageous for applications ranging from drug delivery and theranostics[1,2] to sensing,[3] electronics,[4] and catalysis.[5] Suspending the nanoparticles in solutions maximizes their accessible surface area to take advantage of these novel properties. Maximizing surface area requires that the nanoparticles remain stable and dispersed as individual particles, often in the presence of environmental factors that alter stability such as pH,[6,7] ionic strength,[8] and macromolecular depletants.[9,10] Hence, in many applications the nanoparticle surface is functionalized with surfactants, charged compounds, or macromolecules to induce repulsions between the nanoparticles or favorable chemical interactions with the surrounding solution. In other settings, however, multiparticle assemblies of gold nanoparticles exhibit distinctive and desirable functional properties, such as modified cellular uptake[7,11] or binding and detecting biomolecules.[12] As a second example, percolating nanostructures can improve the thermal or electrical conductivity and optical or mechanical properties of composite materials.[13,14] Tuning the desired functional properties requires control over the assembly of the nanoparticles. Spherical nanoparticles are easily assembled into amorphous aggregates,[15−17] but the production of one- and two-dimensional structures requires patchy functionalization.[18,19] High-aspect-ratio nanorods such as carbon nanotubes can pack into triangular or hexagonal structures,[20−22] and form liquid crystals at modest particle volume fractions.[23,24] Nanoparticles with greater geometric complexity can form a variety of complex superlattice structures due to the directionality of attractive interactions.[25,26] Open fractal structures featuring a hierarchy of length scales are crucial to applications such as additive manufacturing[27] and have been observed for polymer nanocomposites prepared with carbon nanotubes but only at high nanoparticle concentrations.[28] The production of controlled and tunable 3-D structures of anisotropic nanoparticles at low concentrations, however, continues to pose a challenge.

One route to assemble nanoparticles is to induce well-controlled depletion interactions from macromolecules in solution. Polymers added to solution, as one example, have well-defined characteristic length scales (such as the radius of gyration R_g and the correlation length ξ representing the average distance between neighboring chains). Polymer-induced depletion interactions are well-studied for micron-sized colloidal particles,[29] where the polymer chains are much smaller than the colloids, but additional factors alter interactions between nanoscale particles in crowded macromolecular solutions. The simplest theory for depletion interactions, due to Asakura and Oosawa,[30] approximates the polymer coils as noninteracting hard spheres so that the depletant concentration is negligible at the particle surface and

Received: December 1, 2017
Accepted: January 17, 2018
Published: January 17, 2018

DOI: 10.1021/acsanm.7b00277
ACS Appl. Nano Mater. 2018, 1, 877−885

discontinuously increases to the bulk concentration at a distance equal to the depletant radius away from the particle surface. Under this assumption, the interaction potential between particles is proportional to the osmotic pressure of the solution and the volume excluded to the polymer. The flexibility of the polymer chains, however, smooths out the concentration profile of the depletant near the particle surface, and can thus modulate the strength and range of polymer-induced forces.[31] To a first-order approximation, the depletion strength becomes inversely proportional to ξ in semidilute polymer solutions.[32] Furthermore, enthalpic interactions between the polymeric depletants and particles affect the interparticle forces, leading to stronger attraction for unfavorable enthalpic interactions and weaker attraction or even repulsion for favorable particle−polymer interactions.[33] Because nanoparticles are much smaller than colloids, their characteristic length scales are comparable in magnitude to those of the depleting polymer. In this "protein limit,"[34] depletion interactions may exhibit further deviations from the simple Asakura−Oosawa picture,[35,36] instead agreeing with predictions from the polymer reference-interaction site model.[37] These deviations modify the phase behavior of suspensions of nearly spherical nanoparticles,[38−45] but the effect of depletion interactions in the "protein limit" on the assembly of anisotropic particles remains incompletely understood.

Here, we use a well-characterized model system of polymer-grafted gold nanorods (AuNRs) in polymer solutions to investigate the effects of macromolecular crowding on the structure of AuNR aggregates. AuNRs synthesized through a seed-mediated growth method are grafted with short poly(ethylene oxide) (PEO) chains and suspended in semidilute solutions of PEO of varying molecular weight. The optical spectra of these suspensions, arising from localized surface plasmon resonances, exhibit marked shifts as a function of solution PEO size and concentration, consistent with changes in the dispersion of the AuNRs. Small-angle X-ray scattering (SAXS) experiments reveal that the AuNRs aggregate at sufficiently high concentrations of polymer. The characteristic distance between the AuNRs decreases as the concentration of polymer in solution is increased, independent of the molecular weight of the depletant. These changes in structure are consistent with an increase in depletion strength that compresses the grafted brushes, controlled only by the correlation length ξ of polymers in solution. Both the fractal dimension (determined from the low-wavevector slope of the structure factor) and the number of neighbors (assessed semiquantitatively from the ratio of the nearest neighbor peak height) depend nonmonotonically on polymer concentration and hence polymer correlation length ξ, suggesting that the aggregate structure is the result of opposing kinetic processes. The dynamics of nanoparticles in polymer solutions decouple from the bulk viscoelasticity of the polymer solutions and are controlled by the nanoparticle diameter d_{NP} and ξ.[46,47] The dependence of both attraction strength and particle mobility on ξ collapses the structural properties onto a single master curve. Thus, the structure is determined by a competition between the attraction strength and particle transport rate, which, respectively, increase and decrease as ξ decreases, resulting in a transition from reaction-limited to diffusion-limited aggregation with increasing polymer concentration.

MATERIALS AND METHODS

Gold Nanorod Synthesis. Gold nanorods (AuNRs) are synthesized using a seed-mediated growth method.[48] Briefly, a seed solution is prepared by mixing 5 mL of 0.5 mM chloroauric acid ($HAuCl_4$, Sigma-Aldrich) with 5 mL of 0.2 M cetyltrimethylammonium bromide (CTAB, Alfa Aesar) to which 0.6 mL of fresh 0.01 M sodium borohydride ($NaBH_4$, Sigma-Aldrich) solution is added to initiate seed growth. To synthesize the AuNRs, a mixture of 4.5 g of CTAB, 0.55 g of 5-bromosalicylic acid (Alfa Aesar), and 125 mL of water is heated to 70 °C to dissolve the 5-bromosalicylic acid and then cooled to 30 °C for the rest of the reaction. Silver nitrate (6 mL at a concentration of 4 mM, Sigma-Aldrich) is added and left unagitated for 15 min. Next, 125 mL of 1 mM $HAuCl_4$ is added and stirred for 15 min. Finally, 1 mL of 64 mM L-ascorbic acid (Sigma-Aldrich) and 0.4 mL of the seed solution are added, and the reaction mixture is briefly stirred for 30 s before reacting undisturbed for 12 h. The resulting AuNRs are purified by centrifugation, decanting supernatant, and redispersing in fresh water twice. To ensure a neutral interaction between the AuNRs and the poly(ethylene oxide) (PEO) in solution, the purified AuNRs are reacted with 4 g of thiol-PEO (weight-averaged molecular weight M_w = 2 kDa, Nanocs), which covalently bonds to the gold surface, for over 24 h at room temperature. The functionalized AuNRs are repurified using the same method. The dimensions of the functionalized AuNRs are 58 ± 5 nm in length and 17 ± 3 nm in diameter (aspect ratio L/d_{NP} = 3.4 ± 0.7), as measured using transmission electron microscopy (TEM). Due to the low M_w of the thiol-PEO and the high mass of the AuNRs, the thiol-PEO grafting density cannot be determined through traditional methods such as thermal gravimetric analysis. Previous studies,[49,50] however, reported grafting densities for short-chain thiol-PEO of ≈3−4 chains nm^{-2}.

Rheology. Initial polymer stock solutions are prepared by dissolving the appropriate amount of PEO (M_w = 35, 100, 200, 400, or 1000 kDa) in water (Milli-Q, Millipore) and homogenizing on a roll mixer for 2 days. The stock solution is then diluted with additional water and further homogenized for 24 h to produce solutions with the desired polymer concentration. Rheology experiments are performed on a Discovery Hybrid rheometer (DHR-2, TA Instruments) at constant stress in the steady-shear configuration using a Couette geometry with a bob length of 42 mm and diameter of 28 mm. The steady-shear viscosities are measured as a function of shear rate to ensure that the Newtonian zero-shear plateau is reached.

Small-Angle X-ray Scattering. Polymer solutions are prepared as described for rheology experiments. A small amount of a concentrated suspension of AuNRs (volume fraction $\phi \approx 10^{-3}$) is added to the polymer solution and mixed with a vortex mixer for solutions with polymer concentration $c < 10c^*$ or stirred manually until homogeneous for higher concentrations to produce a suspension with a AuNR concentration of $\phi \approx 10^{-5}$. This AuNR concentration is high enough to generate significant scattering intensity but low enough to mitigate interparticle interactions or multiple scattering effects. Prepared solutions are pipetted into 1 mm o.d. quartz capillaries, which are briefly centrifuged to drive the solution to the bottom and then sealed with wax to prevent evaporation. We collect small-angle X-ray scattering (SAXS) data over a wavevector range $0.0019 < Q < 0.08$ Å^{-1}, corresponding to length scales ranging from approximately 10 to 300 nm, at the 8-ID-I beamline at the Advanced Photon Source, Argonne National Laboratory. The 2-D scattering intensities for all solutions are azimuthally uniform and show no signature of alignment or preferred orientation. Thus, the 2-D scattering intensity is azimuthally averaged into a 1-D scattering intensity as a function of scattering wavevector Q.

UV Spectroscopy. The AuNR suspensions used for XPCS and SAXS measurements are diluted further with additional polymer solution for a final AuNR concentration $\phi \approx 10^{-7}$. Solutions with higher AuNR concentrations are too optically dense, precluding measurements of their optical spectra. Optical extinction spectra are collected on a Jasco V-570 spectrophotometer using the neat polymer solution as a reference.

DOI: 10.1021/acsanm.7b00277
ACS Appl. Nano Mater. 2018, 1, 877−885

RESULTS

Characterization of Polymer Solutions. The viscoelastic properties of polymer solutions are dictated by two characteristic length scales: the polymer radius of gyration R_g and the correlation length ξ between chains. In the dilute limit, polymer chains exist as individual Gaussian chains with $R_{g,0} = [M_w/(4/3\pi N_{av}c^*)]^{1/3}$, where M_w is the molecular weight and N_{av} is Avogadro's number. $R_{g,0}$ values are calculated to be 8.5, 16, 24, 36, and 62 nm for M_w = 35, 100, 200, 400, and 1000 kDa PEO, respectively. Above the overlap concentration c^*, the chains interact so that a second length scale ξ develops and scales with concentration according to $\xi = R_{g,0}(c/c^*)^{-\nu/(3\nu-1)}$, where ν = 0.59 is the excluded volume exponent for good solvent conditions (Table S1, Supporting Information). Scaling theory[51] predicts that the bulk zero-shear viscosity of the polymer solutions should collapse onto a single master curve as a function of relative polymer concentration c/c^*, as confirmed for the PEO solutions using bulk rheology (Figure 1). The viscosity of the solutions scales as $\eta - \eta_0 \sim (c/c^*)^2$ until the entanglement concentration c_e, beyond which $\eta - \eta_0 \sim (c/c^*)^{14/3}$. Although the bulk viscosities collapse onto a master curve as a function of relative polymer concentrations, the individual length scales do not (inset to Figure 1). Thus, these polymer solutions have similar bulk viscoelastic properties but substantially different nanoscale structures.

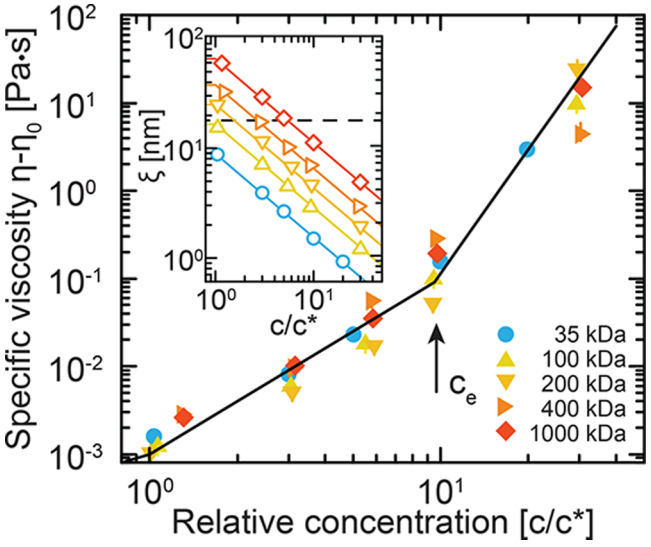

Figure 1. Bulk specific viscosity $\eta - \eta_0$ as a function of relative polymer concentration c/c^* for various PEO molecular weights. Solid lines are scaling predictions[51] with an entanglement concentration $c_e \approx 9.5c^*$. Inset: predicted correlation length ξ for the bulk rheology samples. Dashed line indicates the diameter d_{NP} of AuNRs.

Optical Properties of AuNR Suspensions. The optical properties of AuNRs depend on the shape and dispersion of the gold nanorods. Using optical spectroscopy, we assess the dispersion of the AuNRs in the polymer solutions. Whereas AuNRs used in many previous studies are stabilized with electrostatic charges,[2,6,52] the AuNRs used in this study are covalently functionalized with short 2 kDa PEO chains. With this functionalization, the AuNRs are stable and well-dispersed in water, and the extinction spectrum exhibits two local maxima at wavelengths of 510 and 745 nm, corresponding to the transverse and longitudinal surface plasmon resonances, respectively (Figure 2). Thus, the surface functionalization appears to be uniform across the particle surface, ensuring neutral interactions between AuNRs and the dissolved PEO chains. For AuNRs dispersed in polymer solutions, the spectra change as a function of both polymer M_w and concentration. As the polymer concentration increases, the transverse peak shifts to a higher wavelength of 550 nm, and the longitudinal peak shifts to a lower wavelength of 675 nm. At the highest concentrations of low-M_w polymer, the longitudinal peak broadens so significantly as to nearly disappear. Furthermore, the relative concentration of polymer needed to induce these changes in optical properties becomes progressively larger for polymers of greater M_w.

Previous studies have associated similar changes in optical spectra to the aggregation of AuNRs.[9,53−55] Because the grafted PEO chains have a low M_w, the dissolved chains with much higher M_w do not significantly penetrate the grafted layer.[56−58] Hence, depletion attractions are expected to arise as the dissolved PEO is excluded from a region near the AuNR surface. The changes to the optical spectra confirm that the depletion attractions indeed induce the aggregation of the nanorods. Resuspension of the aggregated AuNRs in water recovers the original optical extinction spectra (Supporting Information, Figure S1), indicating that the aggregation is reversible, as expected for entropic depletion interactions. To support the optical measurements, we obtain quantitative and semiquantitative information on the structure of the AuNR aggregates using small-angle X-ray scattering.

Structural Characterization of AuNR Aggregates. Using SAXS, we assess the structural properties of the AuNR aggregates in these polymer solutions, for which the nanoscale polymer structural length scales are comparably sized to the dimensions of the AuNRs. Although the nanorods are geometrically anisotropic, they orient randomly within the suspension to generate azimuthally isotropic scattering patterns. The azimuthally averaged 1-D SAXS scattering intensity $I(Q)$ exhibits significant changes with increasing polymer concen-

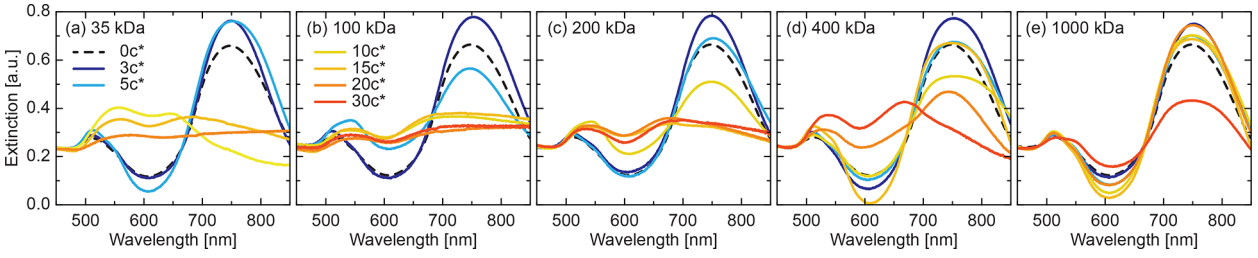

Figure 2. Optical extinction spectra for suspensions of AuNRs in solutions of (a) 35, (b) 100, (c) 200, (d) 400, and (e) 1000 kDa PEO at various concentrations. Curves are shifted vertically to overlap at 450 nm.

DOI: 10.1021/acsanm.7b00277
ACS Appl. Nano Mater. 2018, 1, 877−885

tration (Figure 3). The SAXS intensity for AuNRs dispersed in pure water is well-described by a 1-dimensional cylindrical form factor[59]

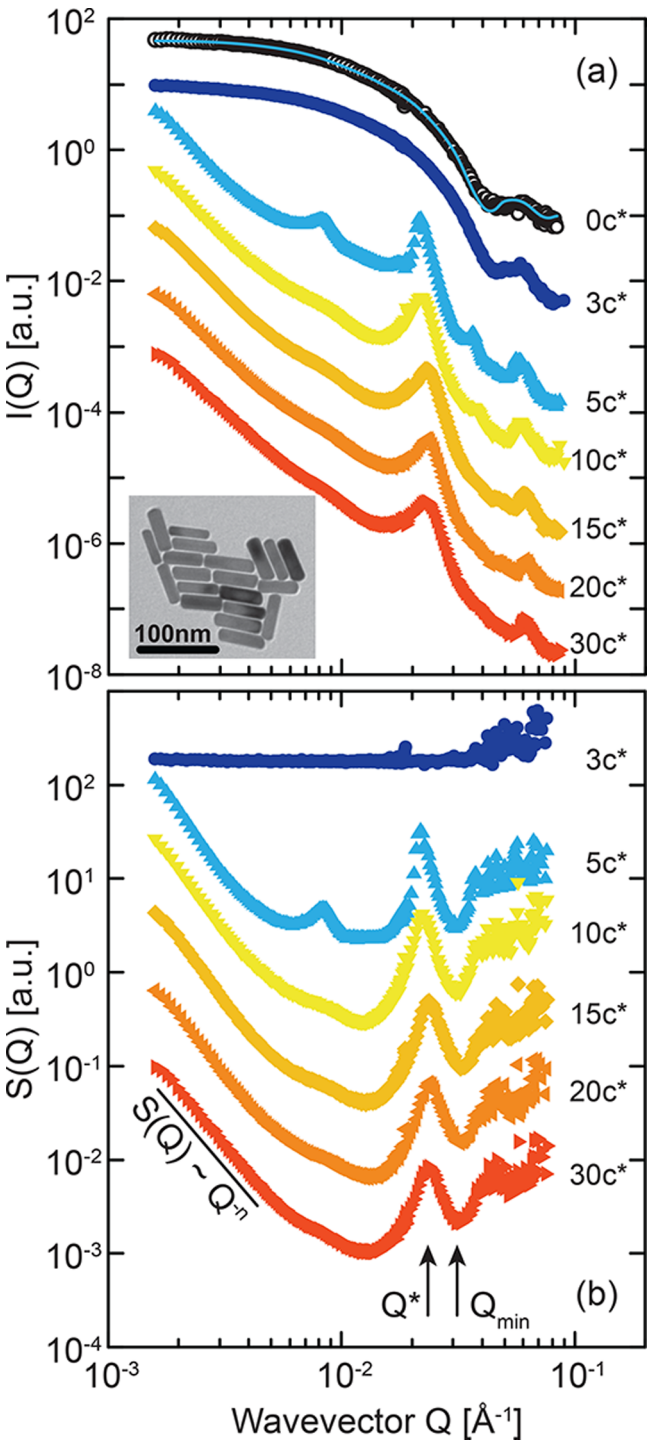

Figure 3. (a) SAXS intensity $I(Q)$ as a function of wavevector Q for AuNRs suspended in aqueous solutions of 100 kDa PEO at various concentrations. Solid curve is fit to cylinder form factor (eq 1). Inset: TEM micrograph of AuNRs grafted with 2 kDa PEO. (b) Structure factor $S(Q)$ as a function of wavevector Q for the same samples. Solid line indicates the low-Q slope n, and arrows indicate wavevectors corresponding to a maximum in $S(Q)$ at Q^* and the first minimum after maximum at Q_{min}. All data are shifted vertically for clarity. SAXS data for remaining depletants shown in the Supporting Information.

$$P(Q) = A\int_0^{\pi/2} f^2(Q, \alpha)\sin(\alpha)\,d\alpha + I_{bkg} \quad (1)$$

where

$$f(Q, \alpha) = \frac{\sin(QL\cos(\alpha)/2)}{QL\cos(\alpha)/2}\frac{J_1(Qd_{NP}\sin(\alpha)/2)}{Qd_{NP}\sin(\alpha)/2} \quad (2)$$

Here, A is a prefactor, α is the angle between the cylinder axis and the wavevector Q, J_1 is the first-order Bessel function of the first kind, and I_{bkg} is a constant background scattering. With this model, the AuNR dimensions are $L = 58 \pm 1$ nm and $d_{NP} = 19 \pm 1$ nm, in good agreement with the dimensions measured using TEM. At low polymer concentrations (i.e., $3c^*$ of 100 kDa PEO), the AuNRs remain well-dispersed. At higher concentrations, however, the AuNRs aggregate, leading to significant scattering intensity *between* AuNRs and the appearance of a structure factor $S(Q)$ (Figure 3b). Even for aggregated samples, the scattering pattern remains isotropic so that $S(Q) = I(Q)/P(Q)$. The Q-dependence of $S(Q)$ contains information about the structure of the aggregates: the primary peak at Q^* is related to the center-to-center distance $d = 2\pi Q^{*-1}$ between nanorods in an aggregate; the ratio $S(Q^*)/S(Q_{min})$ of the structure factor intensity at the primary peak to the first minimum after the peak semiquantitatively captures the number of nearest neighbors within the aggregate and describes the ordering of the nanoparticles. The slope n at low Q captures the mesoscopic fractal dimension of the aggregates.

First, we examine how the center-to-center distance between nanorods changes as a function of depletant M_w and concentration (Figure 4). This interparticle distance is a

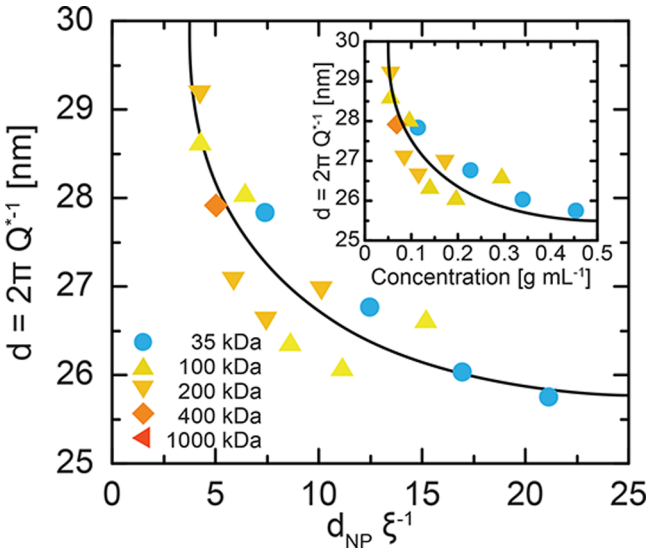

Figure 4. Interparticle distance d as a function of ratio of particle diameter to correlation length $d_{NP}\xi^{-1}$ and (inset) polymer concentration for various PEO molecular weights. Solid curves are guides to the eye.

function of the nanorod diameter and the thickness h of the grafted layer according to $d = d_{NP} + 2h$. At the lowest concentration of polymer that induces aggregation (e.g., $5c^*$ of 100 kDa PEO where $d_{NP}\xi^{-1} \approx 5$), the interparticle distance $d \approx 29$ nm corresponds to cylinders that are packed parallel to each other, as expected from the directionality of the depletion attractions. The resulting grafted thickness at this polymer concentration, $h \approx 5$ nm, is between the size of a free chain in

DOI: 10.1021/acsanm.7b00277
ACS Appl. Nano Mater. 2018, 1, 877−885

good solvent $R_g \approx 1.6$ nm and the contour length $l \approx 13.5$ nm for 2 kDa PEO. As expected for dense polymer brushes, the grafted PEO chains are extended beyond their ideal Gaussian configuration and generate a steric repulsion between the AuNRs. For the 5c^* 100 kDa sample, a second peak in $S(Q)$ appears at $Q \approx 0.009$ Å^{-1}, which approximately corresponds to the length of the nanorods and suggests a hierarchical aggregate structure. Because it does not appear for the other solutions, we do not analyze this peak further. As the ratio d_{NP}/ξ increases, the interparticle distance monotonically decreases, indicating that the grafted layers are more compressed at higher polymer concentrations. Similar compressions have been observed for polymer-grafted spherical nanoparticles[58] or star polymers[56,57] dispersed in solutions of linear polymers. Although analytical expressions for the strength of attraction exist in the spherical colloidal limit,[29] no such expressions exist for anisotropic particles in the protein limit. Nevertheless, we expect that the inverse relationship between depletion strength and ξ holds. Thus, we attribute the decrease in interparticle distance with decreasing ξ to an increase in the strength of the depletion attraction. Additionally, the strength of attraction appears to be dependent only on ξ and independent of depletant M_w.

Although the interparticle distance changes monotonically with ξ, the other two structural measures exhibit pronounced nonmonotonic trends (Figure 5). Previous reports have shown that the height of the primary peak $S(Q^*)$ increases concomitant with the average number of nearest neighbors.[60,61] As the primary peak height $S(Q^*)$ increases, the following minimum $S(Q_{min})$ deepens so that the ratio $S(Q^*)/S(Q_{min})$ increases concomitant with the number of nearest neighbors. Hence, $S(Q^*)/S(Q_{min})$ is a semiquantitative measure of the number of nearest neighbors, and thus the local number density, within an aggregate. $S(Q)$ is required to approach 1 as $Q \rightarrow \infty$. This high-Q limit is not achieved experimentally, however, so estimating the structure factor peak height introduces an arbitrary vertical scaling factor. Alternatively, the number of nearest neighbors can be quantified by converting $S(Q)$ to the pair distribution function $g(r)$ using an inverse Fourier transform and then integrating over the primary peak.[62,63] Reproducing the primary peak in $g(r)$ from such an inversion, however, requires highly accurate measurements at large Q, which are absent for this system. Precisely quantifying the number of nearest neighbors could also be achieved by fitting to an explicit functional form for $S(Q)$, which is common practice for hard sphere suspensions, but such an explicit functional form does not exist for suspensions of anisotropic particles with strong interparticle interactions. Thus, although $S(Q^*)/S(Q_{min})$ is a semiquantitative measure of the number of nearest neighbors, this metric removes error associated with vertically scaling or inverting $S(Q)$ and hence provides a more accurate understanding of how the local number density varies with ξ.

The height of the primary peak in $S(Q)$ (Figure 5a) trends similarly to the ratio $S(Q^*)/S(Q_{min})$ (Figure 5b) as a function of $d_{NP}\xi^{-1}$. We focus on the changes to the ratio $S(Q^*)/S(Q_{min})$, which exhibits a cleaner collapse due to removal of arbitrary vertical scaling. For $d_{NP}\xi^{-1} \lesssim 5$, the absence of a local maximum in $S(Q)$ indicates that the AuNRs remain dispersed in solution; thus $S(Q^*)/S(Q_{min}) = 1$. At higher polymer concentrations, how $S(Q^*)/S(Q_{min})$ varies with $d_{NP}\xi^{-1}$ depends on the depletant M_w (Figure 5b). For the 35 kDa depletant ($R_g < d_{NP}$), the ratio $S(Q^*)/S(Q_{min})$ increases with $d_{NP}\xi^{-1}$, indicating that the number of nearest neighbors in the aggregate increases

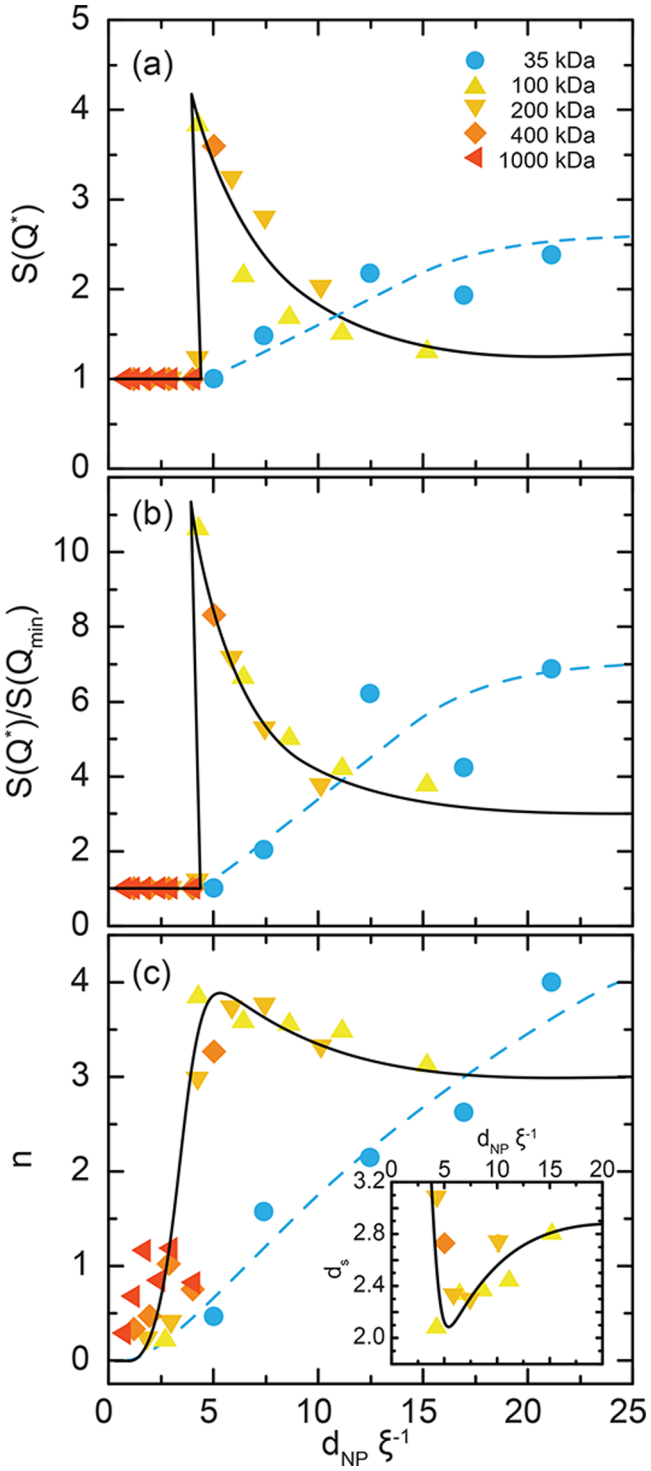

Figure 5. (a) Height of primary peak in $S(Q)$ at $Q = Q^*$. (b) Ratio of peak height to first minimum $S(Q^*)/S(Q_{min})$. (c) Low-Q slope n of the SAXS structure factor as a function of the ratio of nanorod diameter to correlation length $d_{NP}\xi^{-1}$ for various PEO molecular weights. Inset to part c: surface fractal dimension $d_s = 6 - n$ as a function of size ratio $d_{NP}\xi^{-1}$. Dashed blue curves are guides to the eye for the 35 kDa samples. Black curves are guides to the eye for other molecular weights.

with increasing depletion attraction strength. By stark contrast, the ratio $S(Q^*)/S(Q_{min})$ for solutions with larger M_w depletants ($R_g \gtrsim d_{NP}$) discontinuously increases by an order of magnitude when $d_{NP}\xi^{-1} \approx 5$ and then decreases as $d_{NP}\xi^{-1}$ is further

DOI: 10.1021/acsanm.7b00277
ACS Appl. Nano Mater. 2018, 1, 877−885

increased. For these high-M_w depletants, the number of nearest neighbors is maximal at the lowest depletion strength that can still induce aggregation. As the strength of attraction increases, the number of nearest neighbors decreases independently of depletant M_w.

Similar to how the number of nearest neighbors depends on $d_{NP}\xi^{-1}$, the slope n of $S(Q)$ at low Q changes monotonically for the 35 kDa depletant and nonmonotonically for the higher M_w depletants (Figure 5c). At low concentrations, n is clustered between 0 and 1, indicating that there is little to no structuring on long length scales; the absence of a peak in $S(Q)$ at these concentrations indicates that any structures that are formed do not have controlled interparticle spacing. Due to the differences in polymer−particle interactions when the depletant R_g is greater than or less than d_{NP}, the fractal dimensions of the assembled structures vary with depletant M_w. For the 35 kDa depletant, n increases with increasing polymer concentration, indicating that the resulting aggregates are increasingly dense mass fractals. For higher M_w depletants, n attains a maximum when $d_{NP}\xi^{-1} \approx 5$ and ranges from 3 to 4 for all solutions that induce aggregation, indicating that these depletants induce surface fractal structures.[64,65] Thus, n for the higher-M_w depletants can be related to a surface fractal dimension $d_s = 6 - n$ (inset to Figure 5c), which ranges in value from 2 to 3 corresponding to structures with smooth (i.e., dense) and rough interfaces, respectively.[66,67] Based on this change in fractal dimension, the aggregates formed with high-M_w depletants are densest when $d_{NP}\xi^{-1} \approx 5$ and are increasingly rough as the polymer concentration increases.

The nonmonotonic behavior of the fractal dimension and the number of nearest neighbors suggest that the aggregate structure is the result of two opposing kinetic processes. Aggregation in the colloidal size limit depends on the rate and strength with which two colloids bind upon contact and the rate at which they transport toward each other.[16,68] When the bonds are strong, the rate of diffusive transport limits the growth kinetics of the aggregate, termed diffusion-limited aggregation (DLA).[69] In the opposite extreme of weak bonds and fast diffusive transport, the rate of the reaction binding the colloids together restricts the aggregate growth, resulting in reaction-limited aggregation (RLA).[70] RLA aggregates are denser with a larger fractal dimension than those formed by DLA because the colloids within an aggregate are able to rearrange into a more energetically favorable configuration. The strong bonds present in DLA prevent this rearrangement. Although these pictures were originally developed in the colloidal limit with small depletants, we posit that the competition between transport and reaction also shapes depletion-induced aggregates in the protein limit.

DISCUSSION

The balance between the rate of irreversible binding and the rate of transport depends on the strength of the depletion interactions and the nanoparticle diffusivity. By quantifying the monotonic change in interparticle distance (Figure 4), we show that the depletion interaction in the "protein limit" increases in strength as ξ decreases. By contrast, the diffusive transport rate through polymer solutions is expected to decrease along with ξ. Whereas colloidal dynamics couple to the bulk viscoelasticity of the surrounding fluid,[71] nanoparticle dynamics depend sensitively on the nanoparticle size and an effective local viscosity.[46,47] When the diameter of a spherical nanoparticle is comparable to the polymer R_g or ξ in solution, the diffusivity decays as a function of $d_{NP}\xi^{-1}$, although the functional form may be exponential based on hydrodynamic arguments[72−74] or a power law based on scaling arguments.[46] Nevertheless, it is well-established that the diffusive transport of nanoparticles in polymer solutions depends solely on $d_{NP}\xi^{-1}$. Thus, the two processes controlling aggregation of AuNRs when $d_{NP} < R_g$ are both functions only of $d_{NP}\xi^{-1}$ but scale in opposite directions: The strength of the depletion attractions increases, and the AuNR dynamics decrease with decreasing ξ.

To synthesize the changes in various structural properties investigated here, we propose that the aggregation process transitions from RLA to DLA as the depletant concentration is increased. This transition results in the structural assemblies of AuNRs illustrated in Figure 6. At low polymer concentrations

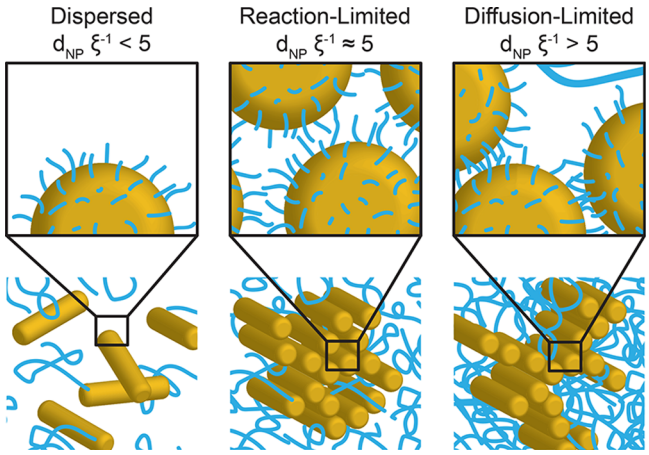

Figure 6. Illustration of the proposed structures formed by the AuNRs in polymer solutions: (left) individually dispersed rods at low polymer concentrations, (middle) dense RLA aggregates with extended grafted brushes at intermediate concentrations, and (right) diffuse DLA aggregates with compressed grafted brushes at high concentrations.

($d_{NP}\xi^{-1} < 5$), the depletion attractions are too weak to induce aggregation, and the AuNRs remain individually dispersed in solution. With the addition of a small amount of polymer so that $d_{NP}\xi^{-1} \approx 5$, the depletion attractions become strong enough to induce aggregation, but the AuNR dynamics are still fast compared to the rate of irreversible binding. Thus, the AuNRs form dense aggregates via RLA with a high number of nearest neighbors and extended grafted layers. At higher concentrations of dissolved polymer ($d_{NP}\xi^{-1} > 5$), stronger attraction forces and slower dynamics lead to DLA, and the resulting aggregates are less dense; each AuNR has fewer nearest neighbors than for aggregates formed at lower concentrations, and the grafted layers are compressed.

The collapse of the structural properties onto a master curve as a function of $d_{NP}\xi^{-1}$ in a depletant system is a unique feature of the "protein limit." In this limit, the bond strength and dynamics are both functions of ξ. By contrast, in the traditional colloidal limit the particle dynamics do not depend on ξ but on the bulk viscosity,[71] which in turn depends on the relative polymer concentration c/c^* (Figure 1). The collapse of structural properties requires d_{NP} to be smaller than the depletant R_g. For the 35 kDa depletant, the nanorod diameter is larger than the depletant R_g, and the resulting aggregate structures are markedly different. The origin of this difference is unclear but may lie in a change in the range of attraction,[75,76] or in different transport properties of the AuNRs when $d_{NP} \gtrsim R_g$.[46]

DOI: 10.1021/acsanm.7b00277
ACS Appl. Nano Mater. 2018, 1, 877−885

The assembly of nanomaterials into larger scale structures in complex environments is a physically rich problem. By using polymer-induced depletion in the "protein limit" and functionalizing the nanoparticle interface with neutrally interacting polymer chains, we isolate the effect of depletant concentration and M_w on structural properties from complicating factors such as charge stabilization or particle−depletant interactions. While this simplified model system allows us to quantify the structural changes that occur during assembly, other systems may have different characteristics that affect structural properties. For example, in the limit of large M_w or low grafting density of the grafted polymer, dissolved polymers may penetrate the grafted layer and thus no longer induce depletion attractions.[56] Additionally, changing the interactions or surface functionalization of the AuNRs will modify the depletion interactions. Attractive interactions between dissolved PEO and the particle surface may greatly reduce the effects of depletion.[77,78] For a charged surface, the long-range electrostatic repulsions will shift the aggregation threshold to higher polymer concentrations, potentially rendering the RLA region inaccessible. These types of interactions, along with particle size and shape, may shift the critical ratio of $d_{NP}\xi^{-1} \approx 5$ at which the depletants induce aggregation. For colloids, the strength of depletion attractions scales proportionally with colloid diameter.[29] We expect this scaling to hold for these anisotropic nanorods. Whereas the structural properties collapse as a function of $d_{NP}\xi^{-1}$, the role of nanorod length is likely more complicated. In the spherical limit where $L = d_{NP}$, the depletion interactions are isotropic, and local anisotropic assembly cannot be achieved. In the opposite limit of infinitely large rods $L \gg d_{NP}$, the rods are kinetically trapped by the surrounding polymer matrix,[28,79] and thus cannot reorient to align in parallel. Between these limits, we expect the physics described here to hold, resulting in a transition between RLA and DLA structures. For longer rods, the depletion interactions should be stronger because of an increase in overlap volume with increasing length, thus shifting the critical $d_{NP}\xi^{-1}$ ratio to lower values. Finally, because the aggregation process is kinetically controlled and therefore path-dependent, solution preparation and processing will likely affect the nanorod structure. As one example, if instead of dispersing the AuNRs directly into polymer solutions the polymer is slowly added to the AuNR suspension, the DLA structures may not form. Although determining the effects of each of these parameters is beyond the scope of this study, they are relevant to many applications and should be considered when targeting specific structures. Nevertheless, this study describes how to prepare nanoparticle assembles *in situ* and characterize their structural properties via scattering. This approach has broad potential for guiding the design of fractal assemblies of anisotropic nanoparticles and their properties in practically relevant environmental conditions.

CONCLUSIONS

The assembly of anisotropic gold nanoparticles into fractal structures with controlled properties is essential for applications in drug delivery, theranostics, sensing, catalysis, and electronics. Here, we demonstrate control over the assembly of anisotropic AuNRs using polymer-induced depletion attractions. Nanorods functionalized with short PEO polymer chains are stable in aqueous suspensions and neutrally interact with dissolved PEO polymers. Because the nanorods and polymers are comparably sized, the depletion forces and transport rates are dependent on the length scale ratio $d_{NP}\xi^{-1}$. The physics controlling the assembly process transitions from reaction-limited at low polymer concentrations (low $d_{NP}\xi^{-1}$) to diffusion-limited at high polymer concentrations (high $d_{NP}\xi^{-1}$), independent of depletant molecular weight. We exploit this change in physics to form structures with controlled interparticle spacing, number density, and fractal dimension.

The production of bulk materials with controlled nanoscale properties limits the deployment of nanotechnology in many applications. Porous nanomaterials demonstrate unique mechanical properties while remaining lightweight,[80] but production of these materials often requires complex and expensive fabrication techniques. Using depletion interactions in the "protein limit" to assemble anisotropic nanoparticles is a facile route to produce open, porous materials in bulk and *in situ* with tunable nanoscale properties. The decoupling of structural properties from the polymer M_w enables the bulk mechanical moduli and nanoscale structures of polymer composites to be independently tuned; varying the molecular weight and grafting density of the grafted polymer grants additional control over the interparticle spacing. Beyond the development of novel materials, the assembly of gold nanoparticles has proven to be beneficial for biosensing[81] and targeted drug delivery by reducing the rate of exocytosis.[7] In addition to generating controlled structures, this study elucidates physics that will improve understanding of the behavior of polymer-grafted nanomaterials in crowded media. Biopolymers and proteins present at volume fractions of up to 40% crowd nanoparticles deployed in biological environments. With *a priori* knowledge of the density or effective correlation length in the cellular cytoplasm or other biological fluids, the nanoparticle dimensions can be varied to generate structures *in vivo* with desired properties.

ASSOCIATED CONTENT

Supporting Information

The Supporting Information is available free of charge on the ACS Publications website at DOI: 10.1021/acsanm.7b00277.

Details on the aggregate reversibility, correlation lengths as a function of depletant M_w and concentration, and additional SAXS data (PDF)

AUTHOR INFORMATION

Corresponding Authors

*E-mail: ramanan@uh.edu.
*E-mail: jcconrad@uh.edu.

ORCID

Ryan Poling-Skutvik: 0000-0002-1614-1647
Ramanan Krishnamoorti: 0000-0001-5831-502X
Jacinta C. Conrad: 0000-0001-6084-4772

Notes

The authors declare no competing financial interest.

ACKNOWLEDGMENTS

We thank Nayoung Park for helpful discussions. This research used resources of the Advanced Photon Source, a U.S. Department of Energy (DOE) Office of Science User Facility operated for the DOE Office of Science by Argonne National Laboratory under Contract DE-AC02-06CH11357. J.C.C. acknowledges support from the Welch Foundation (E-1869).

DOI: 10.1021/acsanm.7b00277
ACS Appl. Nano Mater. 2018, 1, 877−885

REFERENCES

(1) Alkilany, A. M.; Murphy, C. J. Toxicity and Cellular Uptake of Gold Nanoparticles: What We have Learned so Far? *J. Nanopart. Res.* **2010**, *12*, 2313−2333.

(2) Choi, W. I.; Kim, J. Y.; Kang, C.; Byeon, C. C.; Kim, Y. H.; Tae, G. Tumor Regression in vivo by Photothermal Therapy Based on Gold-Nanorod-Loaded, Functional Nanocarriers. *ACS Nano* **2011**, *5*, 1995−2003.

(3) Saha, K.; Agasti, S. S.; Kim, C.; Li, X.; Rotello, V. M. Gold Nanoparticles in Chemical and Biological Sensing. *Chem. Rev.* **2012**, *112*, 2739−2779.

(4) Romo-Herrera, J. M.; Alvarez-Puebla, R. A.; Liz-Marzán, L. M. Controlled Assembly of Plasmonic Colloidal Nanoparticle Clusters. *Nanoscale* **2011**, *3*, 1304−1315.

(5) Thompson, D. T. Using Gold Nanoparticles for Catalysis. *Nano Today* **2007**, *2*, 40−43.

(6) Orendorff, C. J.; Hankins, P. L.; Murphy, C. J. pH-Triggered Assembly of Gold Nanorods. *Langmuir* **2005**, *21*, 2022−2026.

(7) Nam, J.; Won, N.; Jin, H.; Chung, H.; Kim, S. pH-Induced Aggregation of Gold Nanoparticles for Photothermal Cancer Therapy. *J. Am. Chem. Soc.* **2009**, *131*, 13639−13645.

(8) Boles, M. A.; Engel, M.; Talapin, D. V. Self-Assembly of Colloidal Nanocrystals: From Intricate Structures to Functional Materials. *Chem. Rev.* **2016**, *116*, 11220−11289.

(9) Tam, J. M.; Murthy, A. K.; Ingram, D. R.; Nguyen, R.; Sokolov, K. V.; Johnston, K. P. Kinetic Assembly of Near-IR-Active Gold Nanoclusters Using Weakly Adsorbing Polymers to Control the Size. *Langmuir* **2010**, *26*, 8988−8999.

(10) Murthy, A. K.; Stover, R. J.; Borwankar, A. U.; Nie, G. D.; Gourisankar, S.; Truskett, T. M.; Sokolov, K. V.; Johnston, K. P. Equilibrium Gold Nanoclusters Quenched with Biodegradable Polymers. *ACS Nano* **2013**, *7*, 239−251.

(11) Albanese, A.; Chan, W. C. W. Effect of Gold Nanoparticle Aggregation on Cell Uptake and Toxicity. *ACS Nano* **2011**, *5*, 5478−5489.

(12) Schwartzberg, A. M.; Grant, C. D.; Wolcott, A.; Talley, C. E.; Huser, T. R.; Bogomolni, R.; Zhang, J. Z. Unique Gold Nanoparticle Aggregates as a Highly Active Surface-Enhanced Raman Scattering Substrate. *J. Phys. Chem. B* **2004**, *108*, 19191−19197.

(13) Paul, D. R.; Robeson, L. M. Polymer Nanotechnology: Nanocomposites. *Polymer* **2008**, *49*, 3187−3204.

(14) Kumar, S. K.; Krishnamoorti, R. Nanocomposites: Structure, Phase Behavior, and Properties. *Annu. Rev. Chem. Biomol. Eng.* **2010**, *1*, 37−58.

(15) Dimon, P.; Sinha, S. K.; Weitz, D. A.; Safinya, C. R.; Smith, G. S.; Varady, W. A.; Lindsay, H. M. Structure of Aggregated Gold Colloids. *Phys. Rev. Lett.* **1986**, *57*, 595−598.

(16) Lin, M. Y.; Lindsay, H. M.; Weitz, D. A.; Ball, R. C.; Klein, R.; Meakin, P. Universality in Colloid Aggregation. *Nature* **1989**, *339*, 360−362.

(17) Boal, A. K.; Ilhan, F.; DeRouchey, J. E.; Thurn-Albrecht, T.; Russell, T. P.; Rotello, V. M. Self-Assembly of Nanoparticles into Structured Spherical and Network Aggregates. *Nature* **2000**, *404*, 746−748.

(18) Akcora, P.; Liu, H.; Kumar, S. K.; Moll, J.; Li, Y.; Benicewicz, B. C.; Schadler, L. S.; Acehan, D.; Panagiotopoulos, A. Z.; Pryamitsyn, V.; Ganesan, V.; Ilavsky, J.; Thiyagarajan, P.; Colby, R. H.; Douglas, J. F. Anisotropic Self-Assembly of Spherical Polymer-Grafted Nanoparticles. *Nat. Mater.* **2009**, *8*, 354−359.

(19) Kumar, S. K.; Jouault, N.; Benicewicz, B.; Neely, T. Nanocomposites with Polymer Grafted Nanoparticles. *Macromolecules* **2013**, *46*, 3199−3214.

(20) Frank, S.; Poncharal, P.; Wang, Z. L.; Heer, W. A. Carbon Nanotube Quantum Resistors. *Science* **1998**, *280*, 1744−1746.

(21) Baranov, D.; Fiore, A.; Van Huis, M.; Giannini, C.; Falqui, A.; Lafont, U.; Zandbergen, H.; Zanella, M.; Cingolani, R.; Manna, L. Assembly of Colloidal Semiconductor Nanorods in Solution by Depletion Attraction. *Nano Lett.* **2010**, *10*, 743−749.

(22) Park, K.; Koerner, H.; Vaia, R. A. Depletion-Induced Shape and Size Selection of Gold Nanoparticles. *Nano Lett.* **2010**, *10*, 1433−1439.

(23) Song, W.; Kinloch, I. A.; Windle, A. H. Nematic Liquid Crystallinity of Multiwall Carbon Nanotubes. *Science* **2003**, *302*, 1363.

(24) Rai, P. K.; Pinnick, R. A.; Parra-Vasquez, A. N. G.; Davis, V. A.; Schmidt, H. K.; Hauge, R. H.; Smalley, R. E.; Pasquali, M. Isotropic-Nematic Phase Transition of Single-Walled Carbon Nanotubes in Strong Acids. *J. Am. Chem. Soc.* **2006**, *128*, 591−595.

(25) Zanella, M.; Bertoni, G.; Franchini, I. R.; Brescia, R.; Baranov, D.; Manna, L. Assembly of Shape-Controlled Nanocrystals by Depletion Attraction. *Chem. Commun.* **2011**, *47*, 203−205.

(26) Young, K. L.; Personick, M. L.; Engel, M.; Damasceno, P. F.; Barnaby, S. N.; Bleher, R.; Li, T.; Glotzer, S. C.; Lee, B.; Mirkin, C. A. A Directional Entropic Force Approach to Assemble Anisotropic Nanoparticles into Superlattices. *Angew. Chem., Int. Ed.* **2013**, *52*, 13980−13984.

(27) Smay, J. E.; Cesarano, J.; Lewis, J. A. Directed Colloidal Assembly of 3D Periodic Structures. *Langmuir* **2002**, *18*, 5429−5437.

(28) Chatterjee, T.; Jackson, A.; Krishnamoorti, R. Hierarchical Structure of Carbon Nanotube Networks. *J. Am. Chem. Soc.* **2008**, *130*, 6934−6935.

(29) Lekkerkerker, H. N.; Tuinier, R. *Colloids and the Depletion Interaction*; Springer: Dordrecht, Netherlands, 2011; Vol. *833*.

(30) Asakura, S.; Oosawa, F. Interaction between Particles Suspended in Solutions of Macromolecules. *J. Polym. Sci.* **1958**, *33*, 183−192.

(31) Kleshchanok, D.; Tuinier, R.; Lang, P. R. Direct Measurements of Polymer-Induced Forces. *J. Phys.: Condens. Matter* **2008**, *20*, 073101.

(32) de Gennes, P. Colloid Suspensions in a Polymer Solution. *C. R. Seances Acad. Sci., Ser. B* **1979**, *288*, 359−361.

(33) Semenov, A. N.; Shvets, A. A. Theory of Colloid Depletion Stabilization by Unattached and Adsorbed Polymers. *Soft Matter* **2015**, *11*, 8863−8878.

(34) Mutch, K. J.; van Duijneveldt, J. S.; Eastoe, J. Colloid − Polymer Mixtures in the Protein Limit. *Soft Matter* **2007**, *3*, 155−167.

(35) Kulkarni, A.; Chatterjee, A.; Schweizer, K.; Zukoski, C. Depletion Interactions in the Protein Limit: Effects of Polymer Density Fluctuations. *Phys. Rev. Lett.* **1999**, *83*, 4554−4557.

(36) Vivarès, D.; Belloni, L.; Tardieu, A.; Bonneté, F. Catching the PEG-Induced Attractive Interaction between Proteins. *Eur. Phys. J. E: Soft Matter Biol. Phys.* **2002**, *9*, 15−25.

(37) Chatterjee, A. P.; Schweizer, K. S. Microscopic Theory of Polymer-Mediated Interactions between Spherical Particles. *J. Chem. Phys.* **1998**, *109*, 10464−10476.

(38) Wormuth, K. R. Patterns of Phase Behavior in Polymer and Amphiphile Mixtures. *Langmuir* **1991**, *7*, 1622−1626.

(39) Clegg, S. M.; Williams, P. A.; Warren, P.; Robb, I. D. Phase Behavior of Polymers with Concentrated Dispersions of Surfactants. *Langmuir* **1994**, *10*, 3390−3394.

(40) Piculell, L.; Bergfeldt, K.; Gerdes, S. Segregation in Aqueous Mixtures of Nonionic Polymers and Surfactant Micelles. Effects of Micelle Size and Surfactant Headgroup/Polymer Interactions. *J. Phys. Chem.* **1996**, *100*, 3675−3679.

(41) Tuinier, R.; Dhont, J. K.; De Kruif, C. G. Depletion-Induced Phase Separation of Aggregated Whey Protein Colloids by an Exocellular Polysaccharide. *Langmuir* **2000**, *16*, 1497−1507.

(42) Ramakrishnan, S.; Fuchs, M.; Schweizer, K. S.; Zukoski, C. F. Concentration Fluctuations in a Model Colloid-Polymer Suspension: Experimental Tests of Depletion Theories. *Langmuir* **2002**, *18*, 1082−1090.

(43) Ramakrishnan, S.; Fuchs, M.; Schweizer, K. S.; Zukoski, C. F. Entropy Driven Phase Transitions in Colloid-Polymer Suspensions: Tests of Depletion Theories. *J. Chem. Phys.* **2002**, *116*, 2201−2212.

(44) Vliegenthart, G. A.; van Duijneveldt, J. S.; Vincent, B. Phase Transitions and Gelation of Silica-Polystyrene Mixtures in Benzene. *Faraday Discuss.* **2003**, *123*, 65−74.

DOI: 10.1021/acsanm.7b00277
ACS Appl. Nano Mater. 2018, 1, 877−885

(45) Hennequin, Y.; Evens, M.; Quezada Angulo, C. M.; van Duijneveldt, J. S. Miscibility of Small Colloidal Spheres with Large Polymers in Good Solvent. *J. Chem. Phys.* **2005**, *123*, 054906.
(46) Cai, L.-H.; Panyukov, S.; Rubinstein, M. Mobility of Nonsticky Nanoparticles in Polymer Liquids. *Macromolecules* **2011**, *44*, 7853−7863.
(47) Poling-Skutvik, R.; Krishnamoorti, R.; Conrad, J. C. Size-Dependent Dynamics of Nanoparticles in Unentangled Polyelectrolyte Solutions. *ACS Macro Lett.* **2015**, *4*, 1169−1173.
(48) Ye, X.; Jin, L.; Caglayan, H.; Chen, J.; Xing, G.; Zheng, C.; Doan-Nguyen, V.; Kang, Y.; Engheta, N.; Kagan, C. R.; Murray, C. B. Improved Size-Tunable Synthesis of Monodisperse Gold Nanorods Through the Use of Aromatic Additives. *ACS Nano* **2012**, *6*, 2804−2817.
(49) Harder, P.; Grunze, M.; Dahint, R.; Whitesides, G. M.; Laibinis, P. E. Molecular Conformation in Oligo(ethylene glycol)-Terminated Self-Assembled Monolayers on Gold and Silver Surfaces Determines Their Ability To Resist Protein Adsorption. *J. Phys. Chem. B* **1998**, *102*, 426−436.
(50) Rahme, K.; Chen, L.; Hobbs, R. G.; Morris, M. A.; O'Driscoll, C.; Holmes, J. D. PEGylated Gold Nanoparticles: Polymer Quantification as a Function of PEG Lengths and Nanoparticle Dimensions. *RSC Adv.* **2013**, *3*, 6085−6094.
(51) Rubinstein, M.; Colby, R. H. *Polymer Physics*; Oxford University Press: New York, 2003.
(52) Park, S.; Sinha, N.; Hamad-Schifferli, K. Effective Size and Zeta Potential of Nanorods by Ferguson Analysis. *Langmuir* **2010**, *26*, 13071−13075.
(53) Jiang, G.; Hore, M. J. A.; Gam, S.; Composto, R. J. Gold Nanorods Dispersed in Homopolymer Films: Optical Properties Controlled by Self-Assembly and Percolation of Nanorods. *ACS Nano* **2012**, *6*, 1578−1588.
(54) Chen, H.; Shao, L.; Li, Q.; Wang, J. Gold Nanorods and their Plasmonic Properties. *Chem. Soc. Rev.* **2013**, *42*, 2679−2724.
(55) Wang, D.; Hore, M. J. A.; Ye, X.; Zheng, C.; Murray, C. B.; Composto, R. J. Gold Nanorod Length Controls Dispersion, Local Ordering, and Optical Absorption in Polymer Nanocomposite Films. *Soft Matter* **2014**, *10*, 3404−3413.
(56) Stiakakis, E.; Vlassopoulos, D.; Likos, C. N.; Roovers, J.; Meier, G. Polymer-Mediated Melting in Ultrasoft Colloidal Gels. *Phys. Rev. Lett.* **2002**, *89*, 208302.
(57) Wilk, A.; Huißmann, S.; Stiakakis, E.; Kohlbrecher, J.; Vlassopoulos, D.; Likos, C. N.; Meier, G.; Dhont, J. K. G.; Petekidis, G.; Vavrin, R. Osmotic Shrinkage in Star/Linear Polymer Mixtures. *Eur. Phys. J. E: Soft Matter Biol. Phys.* **2010**, *32*, 127−134.
(58) Poling-Skutvik, R.; Olafson, K. N.; Narayanan, S.; Stingaciu, L.; Faraone, A.; Conrad, J. C.; Krishnamoorti, R. Confined Dynamics of Grafted Polymer Chains in Solutions of Linear Polymer. *Macromolecules* **2017**, *50*, 7372−7379.
(59) Guinier, A.; Fournet, G. *Small-Angle Scattering of X-Rays*; John Wiley and Sons: New York, 1955.
(60) Ramsay, J. D.; Booth, B. O. Determination of Structure in Oxide Sols and Gels From Neutron Scattering and Nitrogen Adsorption Measurements. *J. Chem. Soc., Faraday Trans. 1* **1983**, *79*, 173−184.
(61) Svensson, E. C.; Sears, V. F.; Woods, A. D. B.; Martel, P. Neutron-Diffraction Study of the Static Structure Factor and Pair Correlations in Liquid ^{4}He. *Phys. Rev. B: Condens. Matter Mater. Phys.* **1980**, *21*, 3638−3651.
(62) Salmon, P. A Neutron Diffraction Study on the Structure of Liquid Germanium. *J. Phys. F: Met. Phys.* **1988**, *18*, 2345−2352.
(63) Cristiglio, V.; Cuello, G. J.; Piarristeguy, A. A.; Pradel, A. The Coordination Number Calculation from Total Structure Factor Measurements. *J. Non-Cryst. Solids* **2009**, *355*, 1811−1814.
(64) Schaefer, D. W.; Keefer, K. D. Structure of Random Porous Materials: Silica Aerogel. *Phys. Rev. Lett.* **1986**, *56*, 2199−2202.
(65) Hurd, A. J.; Schaefer, D. W.; Martin, J. E. Surface and Mass Fractals in Vapor-Phase Aggregates. *Phys. Rev. A: At., Mol., Opt. Phys.* **1987**, *35*, 2361−2364.
(66) Sinha, S. K. Scattering from Fractal Structures. *Phys. D* **1989**, *38*, 310−314.
(67) Radliński, A. P.; Radlińska, E. Z.; Agamalian, M.; Wignall, G. D.; Lindner, P.; Randl, O. G. Fractal Geometry of Rocks. *Phys. Rev. Lett.* **1999**, *82*, 3078−3081.
(68) Weitz, D. A.; Huang, J. S.; Lin, M. Y.; Sung, J. Limits of the Fractal Dimension for Irreversible Kinetic Aggregation of Gold Colloids. *Phys. Rev. Lett.* **1985**, *54*, 1416−1419.
(69) Witten, T. A.; Sander, L. M. Diffusion-Limited Aggregation, a Kinetic Critical Phenomenon. *Phys. Rev. Lett.* **1981**, *47*, 1400−1403.
(70) Ball, R. C.; Weitz, D. A.; Witten, T. A.; Leyvraz, F. Universal Kinetics in Reaction-Limited Aggregation. *Phys. Rev. Lett.* **1987**, *58*, 274−277.
(71) Squires, T. M.; Mason, T. G. Fluid Mechanics of Microrheology. *Annu. Rev. Fluid Mech.* **2010**, *42*, 413−438.
(72) Cukier, R. I. Diffusion of Brownian Spheres in Semidilute Polymer Solutions. *Macromolecules* **1984**, *17*, 252−255.
(73) Phillies, G. D. J.; Ullmann, G. S.; Ullmann, K.; Lin, T. Phenomenological Scaling Laws for "Semidilute" Macromolecule Solutions from Light Scattering by Optical Probe Particles. *J. Chem. Phys.* **1985**, *82*, 5242−5246.
(74) Cheng, Y.; Prud'homme, R. K.; Thomas, J. L. Diffusion of Mesoscopic Probes in Aqueous Polymer Solutions Measured by Fluorescence Recovery after Photobleaching. *Macromolecules* **2002**, *35*, 8111−8121.
(75) Poon, W. C. Phase Separation, Aggregation and Gelation in Colloid-Polymer Mixtures and Related Systems. *Curr. Opin. Colloid Interface Sci.* **1998**, *3*, 593−599.
(76) Zhang, I.; Royall, C. P.; Faers, M. A.; Bartlett, P. Phase Separation Dynamics in Colloid-Polymer Mixtures: the Effect of Interaction Range. *Soft Matter* **2013**, *9*, 2076−2084.
(77) Carvalho, B. L.; Tong, P.; Huang, J. S.; Witten, T. A.; Fetters, L. J. Adsorption of End-Functionalized Polymers on Colloidal Spheres. *Macromolecules* **1993**, *26*, 4632−4639.
(78) Zhang, X.; Servos, M. R.; Liu, J. Ultrahigh Nanoparticle Stability Against Salt, pH, and Solvent with Retained Surface Accessibility via Depletion Stabilization. *J. Am. Chem. Soc.* **2012**, *134*, 9910−9913.
(79) Fakhri, N.; MacKintosh, F. C.; Lounis, B.; Cognet, L.; Pasquali, M. Brownian Motion of Stiff Filaments in a Crowded Environment. *Science* **2010**, *330*, 1804−1807.
(80) Meza, L. R.; Das, S.; Greer, J. R. Strong, Lightweight, and Recoverable Three-Dimensional Ceramic Nanolattices. *Science* **2014**, *345*, 1322−1326.
(81) Cao, J.; Sun, T.; Grattan, K. T. V. Gold Nanorod-Based Localized Surface Plasmon Resonance Biosensors: A Review. *Sens. Actuators, B* **2014**, *195*, 332−351.

DOI: 10.1021/acsanm.7b00277
ACS Appl. Nano Mater. 2018, 1, 877−885